THE JOURNAL OF BIOLOGICAL CHEMISTRY VOL. 282, NO. 6, pp. 3871–3880, February 9, 2007

Mechanism of Substrate Sensing and Signal Transmission within an ABC Transporter

USE OF A TROJAN HORSE STRATEGY[*] [S]

Received for publication, September 5, 2006, and in revised form, November 30, 2006 Published, JBC Papers in Press, December 12, 2006, DOI 10.1074/jbc.M608480200

Meike Herget[‡1], **Giani Oancea**[‡1], **Susanne Schrodt**[‡2], **Michael Karas**[§], **Robert Tampé**[‡3], **and Rupert Abele**[‡]

From the [‡]*Institute of Biochemistry and* [§]*Institute of Pharmaceutical Chemistry, Biocenter, Goethe-University Frankfurt, Max-von-Laue-Strasse 9, D-60438 Frankfurt am Main, Germany*

By translocating proteasomal degradation products into the endoplasmic reticulum for loading of major histocompatibility complex I molecules, the ABC transporter TAP plays a focal role in the adaptive immunity against infected or malignantly transformed cells. A key question regarding the transport mechanism is how the quality of the incoming peptide is detected and how this information is transmitted to the ATPase domains. To identify residues involved in this process, we evolved a Trojan horse strategy in which a small artificial protease is inserted into antigenic epitopes. After binding, the TAP backbone in contact is cleaved, allowing the peptide sensor site to be mapped by mass spectrometry. Within this sensor site, we identified residues that are essential for tight coupling of peptide binding and transport. This sensor and transmission interface is restructured during the ATP hydrolysis cycle, emphasizing its important function in the cross-talk between the transmembrane and the nucleotide-binding domains. This allocrite sensor may be similarly positioned in other members of the ABC exporter family.

The transporter associated with antigen processing (TAP)[4] plays a prominent role in the antigen-processing pathway via major histocompatibility complex (MHC) class I molecules (1, 2). A fraction of proteasomal degradation products is translocated into the endoplasmic reticulum by the TAP complex and loaded onto MHC class I molecules. Peptide-loaded MHC complexes can pass the endoplasmic reticulum quality control and traffic to the cell surface, where they display their antigenic cargo to cytotoxic T-lymphocytes, which can thereby efficiently recognize and eliminate infected or malignantly transformed cells. TAP belongs to the superfamily of ATP-binding cassette (ABC) transporters, which translocate a very broad spectrum of substrates across membranes (3, 4).

The TAP complex forms a TAP1/TAP2 heterodimer; each subunit contains a transmembrane domain (TMD) followed by a cytosolic nucleotide-binding domain (NBD). The translocation mechanism can be dissected into an ATP-independent peptide binding and an ATP-dependent translocation step (5). TAP1 and TAP2 are required and sufficient for both processes (5, 6). Peptide binding is composed of a fast association step followed by slow structural reorganization of the transport complex (7, 8). Previous studies demonstrated that peptide binding to the TMDs triggers ATP hydrolysis by the NBDs (9, 10). TAP preferentially binds peptides with a length of 8–16 amino acids (5). Using combinatorial peptide libraries, the first three N-terminal and the last C-terminal residues were identified as critical for peptide binding, whereas amino acids between these "anchor" positions do not significantly contribute to the substrate recognition (11). Remarkably, TAP can also bind peptides with large bulky side chains, including cross-linkers, fluorophors, or extended side chains (9, 12, 13). Strikingly, however, sterically restricted peptides that bind but are not transported do not stimulate ATP hydrolysis (9). How the presence and quality of incoming substrate is detected and transmitted to the ATPase domain is one of the key questions in understanding the transport mechanism of ABC exporters. Data on the sensing of bound substrates and signal transmission in ABC transporters, however, remain virtually absent to date.

To identify residues of the TAP complex involved in sensing the quality of bound peptides we developed a Trojan horse approach. Peptide epitopes were modified by a small iron-dependent chemical protease, which can cleave the polypeptide backbone in very close proximity by reactive oxygen species generated by an iron-catalyzed Fenton reaction. By MALDI-TOF MS and cysteine cross-linking, the contact site was mapped to the cytosolic core loop 1 (CCL1) of TAP1. Within this loop, key residues were identified that upon exchange uncouple peptide binding from peptide transport. This transmission interface is structurally reorganized during the ATP-hydrolysis cycle, demonstrating a critical function of this site in the inter-domain cross-talk within the TAP complex.

* This work was supported by the Deutsche Forschungsgemeinschaft (Grant SFB 628, Functional Membrane Proteomics) and the International Max-Planck-Research School for Structure and Function of Biological Membranes (to G. O. and R. T.). The costs of publication of this article were defrayed in part by the payment of page charges. This article must therefore be hereby marked "*advertisement*" in accordance with 18 U.S.C. Section 1734 solely to indicate this fact.

[S] The on-line version of this article (available at http://www.jbc.org) contains supplemental Fig. S1.

[1] Both authors contributed equally to this work.

[2] Present address: Institute of Cardiovascular Physiology, Goethe-University Frankfurt, Theodor-Stern-Kai 7, 60596 Frankfurt am Main, Germany.

[3] To whom correspondence should be addressed. Tel.: 49-69-798-29475; Fax: 49-69-798-29495; E-mail: tampe@em.uni-frankfurt.de.

[4] The abbreviations used are: TAP, transporter associated with antigen processing; ABC, ATP-binding cassette; BABE, (*S*)-1-(*p*-bromoacetamidobenzyl)ethylenediamine tetraacetate; CCL, cytosolic core loop; MALDI-TOF, matrix-assisted laser desorption ionization-time of flight; MS, mass spectrometry; MHC, major histocompatibility complex; NBD, nucleotide-binding domain; TMD, transmembrane domain; mAb, monoclonal antibody; $BM[PEO]_3$, 1,8-Bis-maleimidotriethylene glycol; ATPγS, adenosine 5′-*O*-(thiotriphosphate); AMPPNP, 5′-adenylyl-β,γ-imidodiphosphate.

EXPERIMENTAL PROCEDURES

Materials—Antibodies used were monoclonal and polyclonal anti-TAP1 (mAb 148.3, 1p2) and anti-TAP2 (mAb 435.3) (5, 6, 10, 14). 1,8-Bismaleimidotriethylene glycol ($BM[PEO]_3$) and 1,10-phenanthroline were ordered from Pierce and Sigma, respectively. (*S*)-1-(*p*-Bromoacetamidobenzyl)ethylenediamine tetraacetate (BABE) was synthesized as described (15).

Expression of Human TAP Mutants—The single cysteine TAP1 mutants, Q277C, G282C, N283C, I284C, M285C, S286C, R287C, V288C, and R659C, were generated by ligase chain reaction with the following primers using cysteine-less human TAP1 with a C-terminal His_{10} tag as template (16): Q277C, CCGAATTCTTCCAGTGCAACCAGACCGC; G282C, GCAGAACCAGACCTGCAACATCATGTCC; N283C, CAGAACCAGACCGGCTGCATCATGTCCAGAG; I284C, GACCGGCAACTGCATGTCCAGAG; M285C, GACCGGCAACATCTGCTCCAGAGTCACCGAAG; S286C, GGCAACATCATGTGTAGAGTCACCGAAGA; R287C, GCAACATCATGTCCTGCGTCACCGAAGATAC; V288C, CGGCAACATCATGTCCAGATGCACCGAAGATACG; and R659C, CAAGCCTCTGCCTCAGTACG. Cysteine-less and single-cysteine TAP1 mutants were cloned in the BamH1 and HindIII sites of pFastBac1 (Invitrogen). Wild-type and cysteine-less TAP2 was cloned in the XhoI and SphI sites of pFastBacDual, respectively. The constructs were confirmed by sequencing. Baculovirus generation, virus infection, and protein expression were performed as described previously (10). Co-infections with baculoviruses containing cysteine-less TAP1 mutants and TAP2wt were performed with a multiplicity of infection of five. Infections with baculovirus containing either cysteine-less TAP1 in combination with wt TAP2, or wt TAP1/2 were performed at a multiplicity of infection of three (10, 16). Insect cells (*Spodoptera frugiperda*, *Sf* 9) were grown in Sf900II medium (Invitrogen) following standard procedures (6). TAP-containing microsomes were isolated by a combination of differential and density gradient centrifugation (6). For crude membrane preparation, 5×10^7 cells per ml were resuspended in Tris buffer (10 mM Tris/HCl, 1 mM dithiothreitol, pH 7.4, supplemented with a protease inhibitor mix: 50 μg/ml 4-(2-aminoethyl)benzenesulfonylfluoride hydrochloride, 1 μg/ml aprotinin, 150 μg/ml benzamidine, 10 μg/ml leupeptin, 5 μg/ml pepstatin) and homogenized with a tight glass Dounce homogenizer (Wheaton). Sucrose was added to a final concentration of 250 mM. Nuclei and cell debris were removed by centrifugation at 200 $\times$ *g* for 4 min followed by 8 min at 700 $\times$ *g*. The remaining membranes were pelleted by centrifugation at 100,000 $\times$ *g* for 20 min at 4 °C, washed once, resuspended in phosphate-buffered saline (pH 7.4), snap-frozen in liquid nitrogen, and stored at −80 °C. Protein concentration was determined by MicroBCA (Pierce).

Peptide Synthesis—Peptides were synthesized by solid-phase technique applying conventional Fmoc (*N*-(9-fluorenyl)methoxycarbonyl) chemistry and purified by reversed-phase C_{18} high-performance liquid chromatography. Peptides containing one single cysteine at each position were modified by a 1.5 molar excess of BABE in 20 mM HEPES (pH 7.4) for 2 h at 20 °C, and purified by reversed-phase high-performance liquid chromatography on a C_{18} column (Vydac-218TP510-C_{18} protein and peptide, 10 $\times$ 250 mm). The identity of the peptides was confirmed by MALDI-TOF MS (Voyager-DE, PerSeptive Biosystems).

Peptide Binding Assays—Peptides were labeled with iodine (^{125}I) (7, 10). TAP-containing membranes (25 μg of protein) were incubated with increasing concentrations of radiolabeled peptides in 50 μl of binding buffer (5 mM $MgCl_2$ in phosphate-buffered saline, pH 7.4) for 15 min at 4 °C. Unbound peptides were removed by washing the membranes twice with 100 μl of ice-cold binding buffer using a vacuum manifold with 96-well filter plates (MultiScreen, 0.65 μm of polyvinylidene difluoride membranes, Millipore). Membrane-associated radioactivity was quantified by γ-counting. Background binding was determined in the presence of a 200-fold excess of unlabeled peptide (RRYQKSTEL). To calculate the dissociation constant K_D of the peptides, data were fitted using the Langmuir (1:1) isotherm (Equation 1),

$$B = \frac{B_{max} \times [P]}{K_D + [P]} \quad \text{(Eq. 1)}$$

where B is the amount of specifically bound peptide, and $[P]$ is the peptide concentration. For competition assays, TAP-containing microsomes (50 μg of total protein) were incubated with radiolabeled peptide (RRYQKSTEL, 150 nM) and 15 μM of iron-chelating peptides in the presence or absence of 30 μM $FeSO_4$ and treated as described above.

Peptide Transport Assays—Crude membranes (150 μg of total protein) were resuspended in 50 μl of AP buffer (phosphate-buffered saline, 5 mM $MgCl_2$, pH 7.0) in the presence of 3 mM ATP or ADP. The transport reaction (50 μl) was started by adding 1 μM RRYQNSTC$^{(F)}$L (fluorescein-labeled cysteine) peptide for 3 min at 32 °C and terminated with stop buffer (phosphate-buffered saline, 10 mM EDTA, pH 7.0) on ice. After centrifugation, the membranes were solubilized in lysis buffer (50 mM Tris/HCl, 150 mM NaCl, 5 mM KCl, 1 mM $CaCl_2$, 1 mM $MnCl_2$, 1% Nonidet P-40, pH 7.5) for 20 min on ice. N-core-glycosylated, therefore transported, peptides were recovered with concanavalin A-Sepharose beads (Sigma) overnight at 4 °C. After washing with lysis buffer, glycosylated peptides were eluted with methyl-α-D-mannopyranoside (200 mM) and quantified with a fluorescence plate reader ($\lambda_{ex/em}$ = 485/520 nm, Polarstar Galaxy, BMG Labtech, Offenburg, Germany).

To measure TAP-dependent transport in whole cells, insect cells (2.5×10^6) were semipermeabilized with 0.05% saponin (Sigma) for 1 min at 25 °C in 200 μl of AP buffer. After washing, the cells were resuspended in a final volume of 100 μl of AP buffer containing ATP (10 mM). The transport reaction was initiated by adding 0.50 μM fluorescent peptide RRYQNSTC$^{(F)}$L for 3 min at 32 °C and terminated with stop buffer on ice. After centrifugation, the cells were solubilized in lysis buffer for 60 min on ice, and N-core-glycosylated peptides were purified and quantified as described above.

Cleavage by Iron-chelating Peptides—Iron-chelating peptides (7.5 μM) were incubated with 2-fold molar excess of $FeSO_4$ in reaction buffer (20 mM HEPES, 140 mM NaCl, 15% glycerol, pH 7.4) just before the experiment. EDTA was added to a final

concentration of 30 μM to remove the excess of weakly bound iron. TAP-containing membranes (25 μg of protein) were added to a total volume of 50 μl and incubated for 15 min at 4 °C. After peptide binding, the cleavage reaction was initiated by addition of ascorbic acid (adjusted to pH 7.4) and H_2O_2 (20 mM final concentration, each). After incubation for 1 min at 22 °C, the reaction was quenched by dithiothreitol (5 mM) and analyzed by SDS-PAGE (10%) and immunoblotting.

Mass Spectrometry—After cleavage (0.5 mg of protein in 500 μl of reaction buffer), membranes were pelleted at 20,000 × *g* and 4 °C for 8 min. TAP was solubilized in reaction buffer containing 35 mM Fos-Choline-14 (Anatrace) for 20 min at 4 °C. Insoluble material was removed by centrifugation at 100,000 × *g* for 30 min at 4 °C. The supernatant was incubated with nickel-nitrilotriacetic acid beads (Qiagen) for 45 min at 4 °C. After three washing steps and subsequent elution with 200 mM imidazole, the samples were precipitated with $CHCl_3$/MeOH (17). Precipitated proteins were solubilized in 2:3 (v/v) hexafluoroisopropanol/formic acid (90%). The matrix 2,5-di-hydroxybenzoic acid was dissolved to saturation in the same solvent. 1 μl of the matrix solution was mixed with 1 μl of sample solution on the MALDI target plate and dried by air stream. Mass spectra were obtained using a MALDI-TOF mass spectrometer (Voyager-DE, PerSeptive Biosystems).

Cysteine Cross-linking—TAP-containing membranes (0.5 mg of protein) were incubated with 1.25 μM of radiolabeled peptide RRYQKCTEL in 200 μl of phosphate-buffered saline for 15 min at 4 °C. Experiments were performed in the presence or absence of competitor peptide (250 μM RRYQKSTEL). Chemical cross-linking was initiated by adding of $BM[PEO]_3$ (0.2 mM final). After incubation for 45 min at 4 °C, the reaction was quenched with dithiothreitol (5 mM). Membranes were washed in reaction buffer and collected by centrifugation at 20,000 × *g* for 8 min at 4 °C. Purification of cross-linked TAP was carried out via nickel-nitrilotriacetic acid beads as described before. For oxidative cross-linking, TAP-containing membranes and radiolabeled RRYQKCTEL were incubated with copper phenanthroline (1 mM $CuSO_4$/4 mM 1,10-phenanthroline) for 5 min at 4 °C under the same conditions as described above. The reaction was stopped by addition of *N*-ethylmaleimide (5 mM) and purified as stated above. TAP was analyzed by SDS-PAGE (10%), and cross-linked products were detected by autoradiography with a PhosphorImager 445i (Molecular Dynamics).

AlF_x Trapping of the TAP Complex—TAP-containing membranes (0.5 mg of total protein) were preincubated with 1 μM RRYQKSTEL in 500 μl of trapping buffer (phosphate-buffered saline, 5 mM ATP, 3 mM $MgCl_2$, 2.5 mM $AlCl_3$, 250 mM NaF) for 25 min at 27 °C. Afterward, membranes were washed in ice-cold trapping buffer, collected by centrifugation at 20,000 × *g* for 8 min at 4 °C, and resuspended in 100 μl of trapping buffer for oxidative cross-linking, peptide transport, or peptide binding (see above).

RESULTS

Peptides Modified by a Chemical Protease Bind Specifically to TAP—To identify residues within the TAP complex sensing incoming peptides, we developed a Trojan horse approach, where each position of the human leukocyte antigen-B27-restricted epitope RRYQKSTEL was modified by a small chemical protease via a single cysteine residue (C1- to C9-peptide, Fig. 1*A*). We first analyzed the TAP binding affinity of these iron-chelating peptides. For the chelating C6-peptide (RRYQKC$^{(BABE)}$TEL), a dissociation constant K_D of 62 ± 16 nM and 118 ± 33 nM was determined in the presence and absence of iron, respectively (Fig. 1*B*). Peptide binding is reduced to background in the presence of an excess of the epitope RRYQKSTEL, which has an affinity of 150 nM (13). These results demonstrate that peptides modified by the chemical protease bind specifically and with

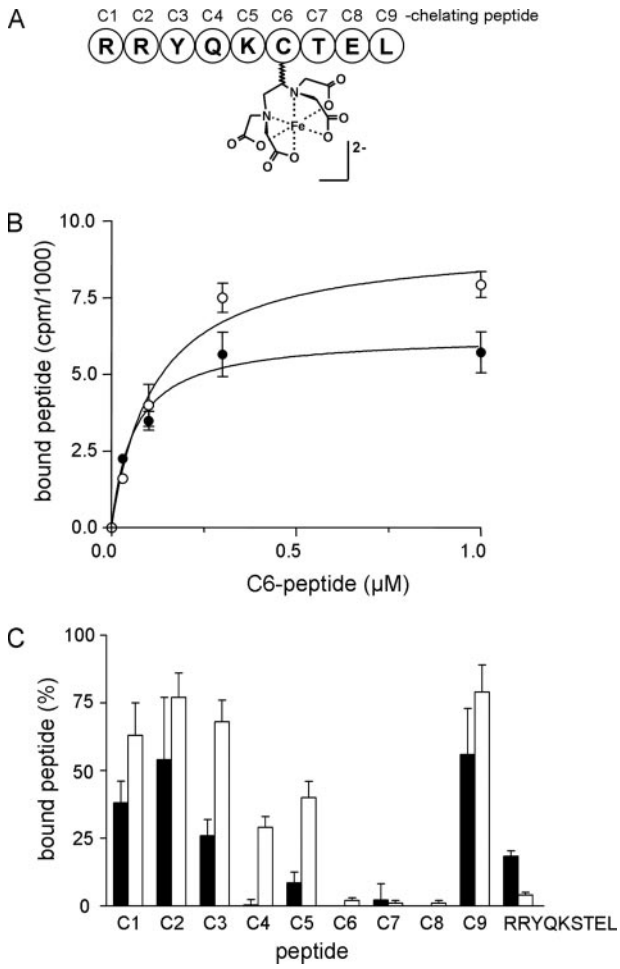

FIGURE 1. **Peptides modified by a chemical protease bind specifically to TAP.** *A*, structure of peptides modified by the artificial iron-dependent protease, BABE. Each residue of the peptide RRYQKSTEL was substituted by cysteine and labeled by the chemical protease. *B*, binding affinity of the iron-chelating C6-peptide. To determine the binding affinity to TAP, increasing concentrations of the radiolabeled chelating C6-peptide were incubated with TAP(wt)-containing membranes at 4 °C for 15 min. The chelating C6-peptide was analyzed in the absence (*open symbols*) or the presence of iron (equimolar ratio of iron and peptide, *filled symbols*). The amount of specifically bound peptide was plotted against peptide concentration and fitted by a Langmuir (1:1) isotherm. The affinity constants were 62 ± 18 nM and 118 ± 33 nM for the iron-loaded and iron-free states, respectively. *C*, binding of peptides modified at different positions (C1 to C9) by the chemical protease was compared by competition assays. TAP(wt)-containing microsomes were incubated with 150 nM of radiolabeled peptide (RRYQKSTEL) and 15 μM of iron-chelating peptide or unlabeled RRYQKSTEL in the presence (*filled symbols*) and the absence (*open symbols*) of 30 μM $FeSO_4$ for 15 min at 4 °C. Specific binding of the reporter peptide was normalized to 100% in the absence of the competitor. All data and errors were derived from triplicate measurements.

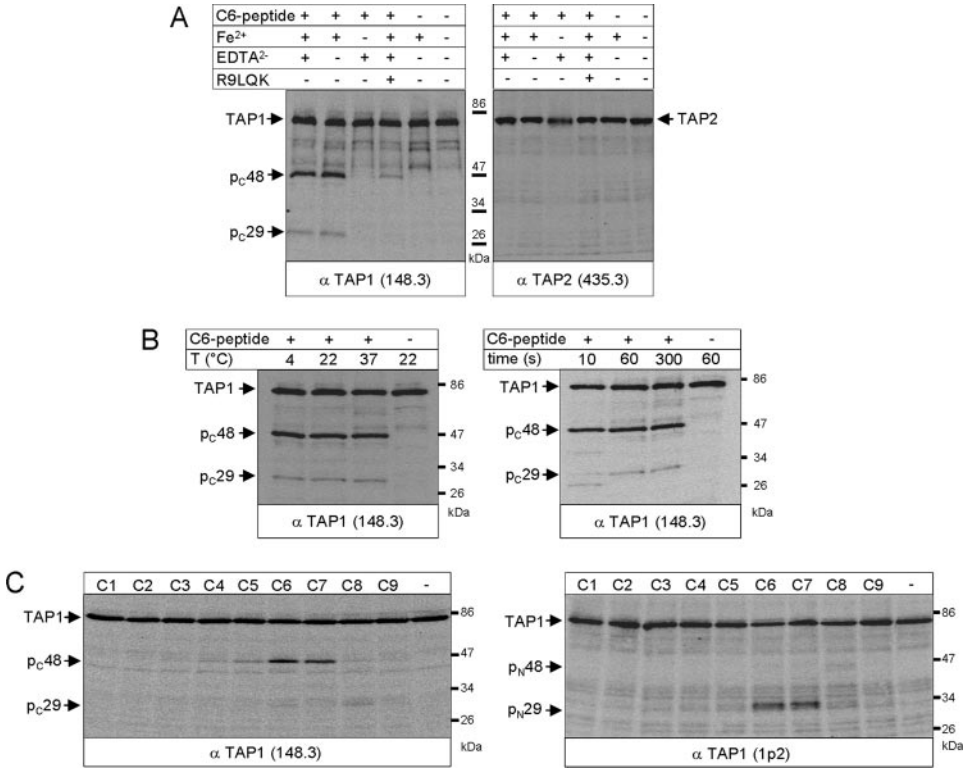

FIGURE 2. **Specific cleavage of TAP1 by iron-chelating peptides.** *A*, cleavage specificity. TAP(wt)-containing membranes (25 μg of total protein) were incubated in the presence or absence of iron-chelating C6-peptide (7.5 μM). $FeSO_4$ (15 μM) and competitor peptide (RRYQKSTEL, 1.5 mM) were added as indicated. EDTA (30 μM) was included to remove weakly bound iron. The cleavage reaction was initiated by addition of ascorbic acid and H_2O_2 (20 mM each) for 60 s at 22 °C. After quenching, TAP cleavage was analyzed by SDS-PAGE and immunoblotting with mAb 148.3 directed against the C terminus of TAP1 and with mAb 435.3 directed against an epitope located in the nucleotide-binding domain of TAP2. *B*, temperature- and time-dependent cleavage. The cleavage reaction was performed at different temperatures for 60 s as described under "Experimental Procedures." Cleavage kinetics by the iron-chelating C6-peptide was analyzed at 22 °C. As control, TAP was incubated with the same concentration of ascorbic acid and H_2O_2 for 60 s in the absence of chelating peptide. *C*, position-specific and asymmetric cleavage of TAP1 by iron-chelating peptides. The cleavage reaction was performed with all nine peptides modified at position C1 to C9 by the chemical protease. The fragments generated by specific cleavage were analyzed by SDS-PAGE and immunoblotting using antibodies directed to different epitopes of TAP1, which are depicted in Fig. 3*C* (−, no cleavage reaction).

high affinity to TAP. We next analyzed the influence of the chemical protease linked at different positions by competition assays using the epitope RRYQKSTEL as reporter (Fig. 1*C*). Attachment of the chemical protease at positions one to three, or position nine decreased the affinity for TAP, whereas peptides modified at positions four to eight bound with affinity similar to that of the original epitope. These results are in perfect agreement with the binding motif of human TAP (11). All chelating peptides show a higher affinity for TAP in the iron-loaded than in the unloaded state. This can be explained by reduced electrostatic repulsion upon complex formation with iron (reduction of negative charges).

Trojan Horse Peptides Cleave the TAP Complex Asymmetrically—After specific binding of Trojan horse peptides to TAP, we initiated a Fenton reaction by addition of hydrogen peroxide and ascorbic acid. This leads to the generation of reactive oxygen species, which can cleave the polypeptide backbone of TAP directly at the contact interface (18). EDTA was added to remove free or weakly bound iron. As shown in Fig. 2*A*, the bound C6-peptide generated C-terminal fragments of TAP1 of 48 kDa (p_C48) and a less prominent of 29 kDa (p_C29) (epitopes and cleavage sites are depicted in Fig. 3*C*). Additional C-terminal cleavage fragments of an apparent molecular mass between 35 and 40 kDa could be detected with low and varying intensities. No TAP cleavage was observed in the absence of either iron or iron-chelating peptides. Most importantly, TAP cleavage was inhibited by an excess of the unmodified peptide epitope, demonstrating that cleavage is specific and origins from peptides specifically bound to the TAP heterodimer. High concentrations of glycerol (20%), which quenches diffusive oxygen species, did not affect the cleavage reaction (data not shown), indicating that cleavage occurs at a direct contact site within the TAP complex. Remarkably, under all conditions examined, we did not observe cleavage of TAP2. We further screened for optimal cleavage by varying temperature and time. Almost the same cleavage pattern of TAP1 was observed at 4, 22, and 37 °C (Fig. 2*B*). Importantly, the TAP1 fragment p_C48 was generated within 10 s, whereas the fragment p_C29 was produced within the first minute at 22 °C. Based on these results, all subsequent cleavage assays were performed for 1 min at 22 °C. Taken together, the iron-chelating peptide bound to the TAP complex causes specific and rapid cleavage of TAP1.

We next examined the TAP-peptide interface in more detail by scanning the chemical protease through various positions (Fig. 2*C*). Strikingly, the C-terminal TAP1 fragment p_C48 was detected only when the chemical protease was placed at positions C4 to C8, with highest cleavage efficiency for the C6- and C7-peptides. In the case of the 29-kDa fragment (p_C29), maximum cleavage efficiency was detected for the C8-peptide. The cleavage pattern did not change by using antibodies specific to other epitopes downstream of TM4 (data not shown). The corresponding N-terminal fragment p_N29 (29 kDa) and less prominent fragment p_N48 (48 kDa) were, however, detected when antibody 1p2 was used, which is specific for an epitope following TM2 of TAP1 (see Fig. 3*C*). Remarkably, we did not observe cleavage of TAP2 by any of the iron-chelating peptides, although the peptide is anchored by both TAP subunits (5). Altogether, these results demonstrate that the iron-chelating peptide cleaves in a position-dependent and asymmetric manner in TAP1. The lack of TAP cleavage in case of peptides carrying the chemical protease at anchor positions can be explained by a decreased binding affinity or a different environment as compared with other positions of the peptide. The

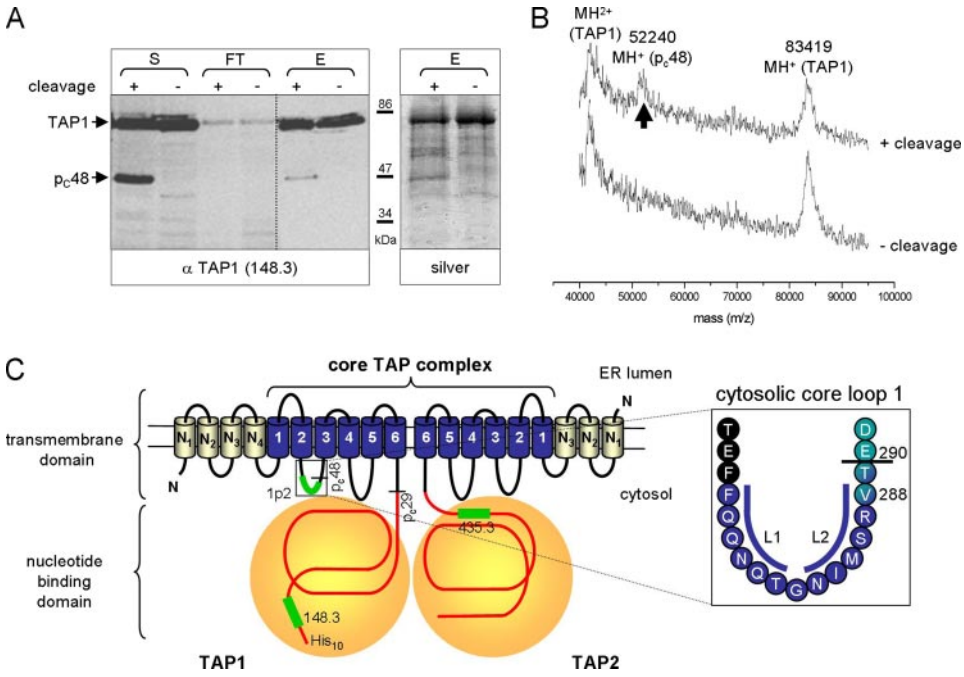

FIGURE 3. **Identification of the peptide contact site by mass spectrometry.** *A*, isolation of the cleavage products. After cleavage, the TAP complex containing cysteine-less TAP1-His_{10}/TAP2(wt) was purified by metal-affinity chromatography. Aliquots of Fos-Choline-14 solubilized protein (*S*), flow-through (*FT*), and eluate of the nickel-nitrilotriacetic acid column (*E*) were analyzed by SDS-PAGE (10%) followed by silver staining and immunoblotting. *B*, MALDI-TOF MS analysis of cleavage products. After purification and precipitation, the pellet was solubilized and analyzed by MADLI-TOF MS. The peaks at 83,419 ± 210 and 52,240 ± 131 Da correspond to full-length TAP1 and cleaved TAP1 p_c48 fragment, respectively. From the molecular mass of the pc48 fragment the cleavage site was assigned to residue 290 ± 2 of TAP1. The peak at 41,703 ± 105 Da reflects the double charged full-length TAP1 (MH^{2+}). As control, TAP was purified without cleavage and analyzed under identical conditions. *C*, model of the contact site within the TAP complex. N-terminal domains and the 2 × 6 TM core of the transmembrane domain of TAP are depicted in *gray* and *blue cylinders*, respectively (41). Based on the unique organization of the TAP-TMD (16) composed of a functional core complex and extra N-terminal domains, the contact site is located in CCL1. The epitopes of mAb 148.3, 1p2, and mAb 435.3 are depicted as *green boxes*, and the cleavage sites are marked by a *line*. The *inset* shows the peptide contact and sensor site at residue 290 ± 2 of TAP1. The arrangement of the L1 and L2 helices is as found in BtuC (21).

cleavage pattern reveals contact sites in the CCL1 and between TM6 and the NBD. To very low extent also cleavage in CCL2 between TM4 and TM5 can be detected.

The Peptide Contact Site Is Identified by Mass Spectrometry—To identify the peptide sensor site, the TAP complex was solubilized by disruptive detergents, purified by metal affinity chromatography (Fig. 3*A*), and analyzed by MALDI-TOF MS (Fig. 3*B*). As internal control, samples with and without cleavage were treated identically. Under cleavage conditions, an extra peak was observed at 52,240 ± 131 Da corresponding to the fragment p_C48. According to the mass resolution, the cleavage site in TAP1 was assigned to residue 290 ± 2. This results in a C-terminal fragment of 52,323 Da, taking cysteine-less TAP1 with an additional affinity tag (LVPRGSGGH$_{10}$) into account for mass calculation. The contact site is located in the CCL1 between TM2 and TM3 (Fig. 3*C*). The peaks detected under both conditions (with and without cleavage) correspond to full-length TAP1 (MH^+ 83,419 ± 210 Da). The peak of doubly charged ions confirms this result. The experimental mass is in perfect agreement with the theoretical mass of 82,998 Da for full-length TAP1. Attempts to isolate and identify the less prominent cleavage fragments failed because of their low amount.

Residue 288 of TAP1 Is in Contact with the Bound Peptide—To provide independent proof for the identified peptide contact interface we established a cross-linking approach with TAP1 mutants and peptides, each containing a single cysteine. After binding of radiolabeled peptides to TAP, membranes were incubated with the thiol-specific cross-linker BM[PEO]$_3$, which has similar dimensions as the chemical protease. Cross-linking products were analyzed by SDS-PAGE and autoradiography. As shown in Fig. 4*A*, specific cross-linking was detected only if a single cysteine (V288C) was placed at the peptide contact site identified by mass spectrometry (see Fig. 3*C*). Background labeling was observed in the presence of an excess of the epitope, demonstrating the specificity of the cross-linking. No cross-linking was monitored for cysteine-less TAP1. TAP1 mutants with single cysteines placed in the NBD (R659C) or N-terminal from the sensor site (F265C) did not show specific cross-linking (Figs. 4*A* and 5C).

To prove the direct contact of the sensor region with the bound peptide, we also performed oxidative cross-linking of single-cysteine TAP and peptides with copper phenanthroline, which induces disulfide formation only if two cysteines are in very close proximity (19). After quenching of free cysteines with NEM, cross-linking products were analyzed by non-reducing SDS-PAGE and autoradiography. Notably, the bound C6-peptide was cross-linked to the TAP1 contact site identified by mass spectrometry, including position 288 (Fig. 4*B*). The cysteine-less and TAP1-R659C mutant did not show a specific cross-linking. Collectively, these results demonstrate that the bound peptide is in direct contact with residue 288 of the CCL1 of TAP1.

Structural Flexibility of the Sensor Interface in TAP1—To generalize our findings, we next investigated whether peptides, which differ in sequence and length, share the same sensor site. Cleavage was therefore performed with 9-, 11-, and 15-mer peptides harboring the chemical protease at the central position. Interestingly, all peptides showed the same cleavage pattern of TAP with a pronounced p_c48 TAP1 fragment and a p_c29 fragment (Fig. 4*C*). Additionally, C-terminal fragments of 35 and 40 kDa were detected. However, none of these peptides induced a cleavage in TAP2 (data not shown). The direct contact with the side chain of the bound peptide was proven by oxidative cysteine cross-linking. All three peptides are specifically cross-linked to residue 288 of TAP1 (Fig. 4*D*). The

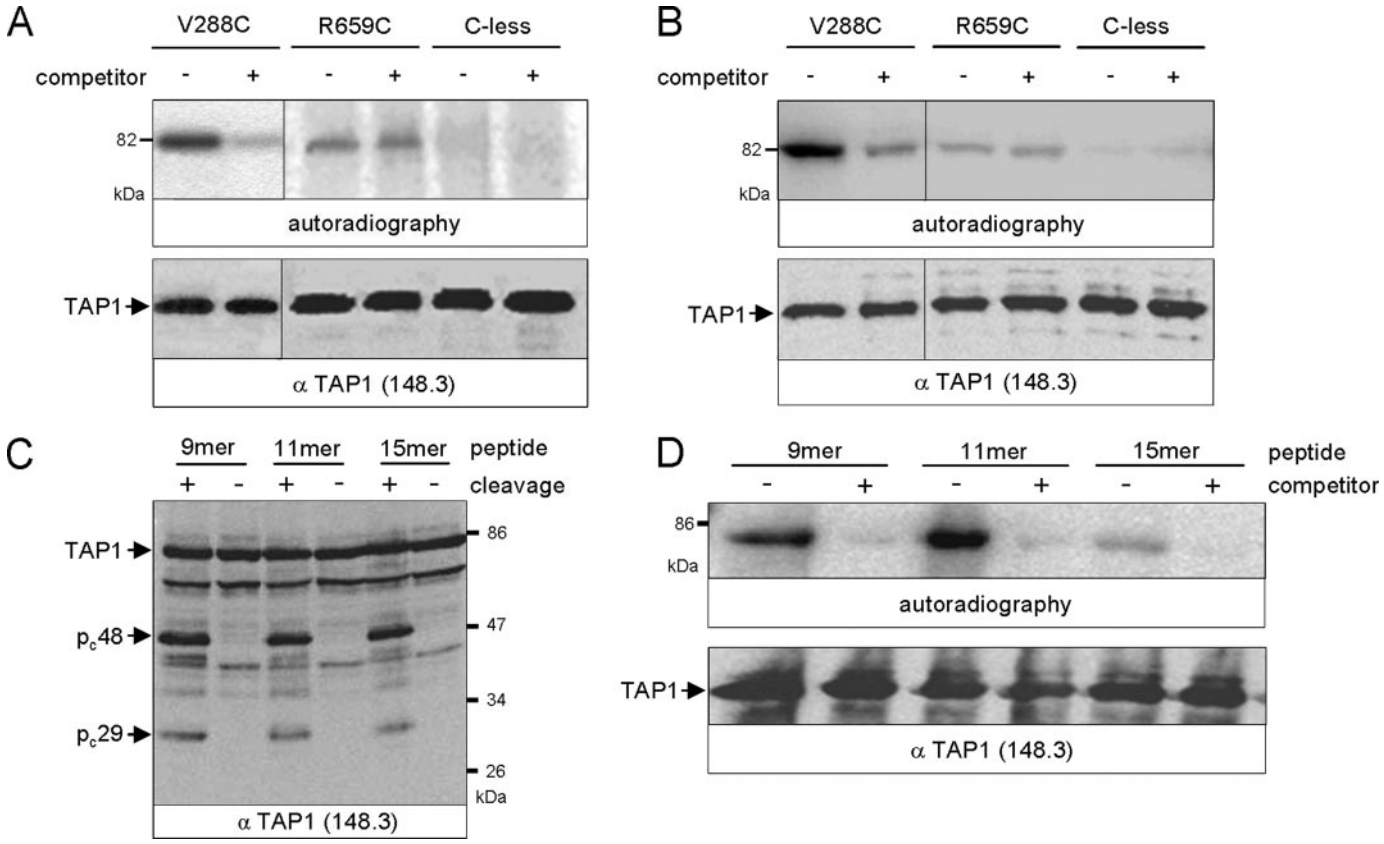

FIGURE 4. **Bound peptides are in direct contact with the cytosolic core loop 1 of TAP1.** *A*, site-specific thiol cross-linking with $BM[PEO]_3$. TAP-containing membranes (0.5 mg of total protein; TAP1 (single cysteine or cysteine-less) combined with TAP2(wt)) were preincubated with radiolabeled C6-peptide (1.25 μM) in the absence or presence of the peptide RRYQKSTEL (250 μM). Cross-linking was induced by adding 0.2 mM of $BM[PEO]_3$. After purification of TAP via metal affinity beads, cross-linked products were analyzed by reducing SDS-PAGE and autoradiography. *B*, oxidative cysteine cross-linking with copper phenanthroline. Experiments were performed as described in *A*, except that membranes were incubated with copper phenanthroline (1 mM) and SDS-PAGE was performed under non-reducing conditions. Equal amounts of TAP in each experiment were confirmed by immunoblotting. *C*, flexibility of the peptide contact site probed by chelating peptides of increasing length. TAP(wt)-containing membranes (25 μg of total protein) were incubated in the presence of 7.5 μM of iron-chelating 9-mer (RRYQKCTEL), 11-mer (RRYQKCNSTEL), or 15-mer (RRYQKLTCAVNSTEL) and $FeSO_4$ (15 μM). The cleavage reaction was initiated by addition of ascorbic acid and H_2O_2 (20 mM each) for 60 s at 22 °C. After quenching, TAP cleavage was analyzed by SDS-PAGE and immunoblotting with mAb 148.3. *D*, direct contact of peptides of different length with the peptide sensor site. Site-specific oxidative cross-linking with 9-mer, 11-mer, and 15-mer peptides was performed and analyzed as indicated in Fig. 4*B* using TAP1(V288C)/TAP2(wt).

decreased cross-linking efficiency for the 15-mer peptide seems to result from the more than 10-fold lower binding affinity (> 8 μM) as the shorter peptides (9-mer 0.30 μM, 11-mer 0.69 μM, and data not shown). In summary, all peptides irrespective of their length bind with the same orientation to TAP, and the central part between the N- and C-terminal peptide anchor positions is in contact with the sensor interface.

The Sensor Interface in TAP1 Is Essential for Peptide Transport—Remarkably, the identified sensor site within CCL1 shares some degree of homology with intracellular domain 1 of the bacterial lipid A exporter MsbA and the L-loop of the bacterial vitamin B_{12} importer (Fig. 5*A*). Based on the x-ray structure of these proteins (20, 21), these loops form the major contact between the transmembrane domain and the Q-loop and the α-helical subdomain of the nucleotide-binding domain as derived from distance measurements. To elucidate the functional role of residues within the identified sensor loop of TAP1, we applied a cysteine-scanning approach. Remarkably, all single cysteine mutants showed similar peptide binding (Fig. 5*B*). In contrast, mutations of the most conserved residues within the sensor loop (Gly-282, Ile-284, and Arg-287) strongly decreased peptide transport (Fig. 5*B*). In these mutants, the coupling between peptide binding and transport is disrupted, indicating that this sensor site serves as a checkpoint in controlling downstream events. Mainly residue 288 can be cross-linked with the C6-peptide. In addition, the TAP1 mutants I284C and S286C are cross-linked to a very small extend. All other residues within the transmission interface are not in contact with the bound peptide (Fig. 5*C*). Taken together, we propose a dual function of the contact site as peptide sensor and signal transducer.

The Peptide Sensor Interface Is Restructured in the Transition State of the ATPase Domains—Peptide transport by TAP is a multistep process composed of peptide binding, signal transmission, and peptide translocation. To elucidate structural changes in the peptide sensor and transmission interface, we examined the peptide-TAP1 contact site at various stages of the ATP hydrolysis cycle. To fix each single state, we performed this experiment at 4 °C where ATP hydrolysis is absent. Apart from an ATP-bound, ADP-bound, and nucleotide-free situation, a catalytic transition state can be arrested by aluminum fluoride. AlF_x is a potent ATPase inhibitor, which replaces the γ-phosphate of ATP and traps ADP stably in the ATP binding pocket of TAP (10) and also other ATPases like P-glycoprotein

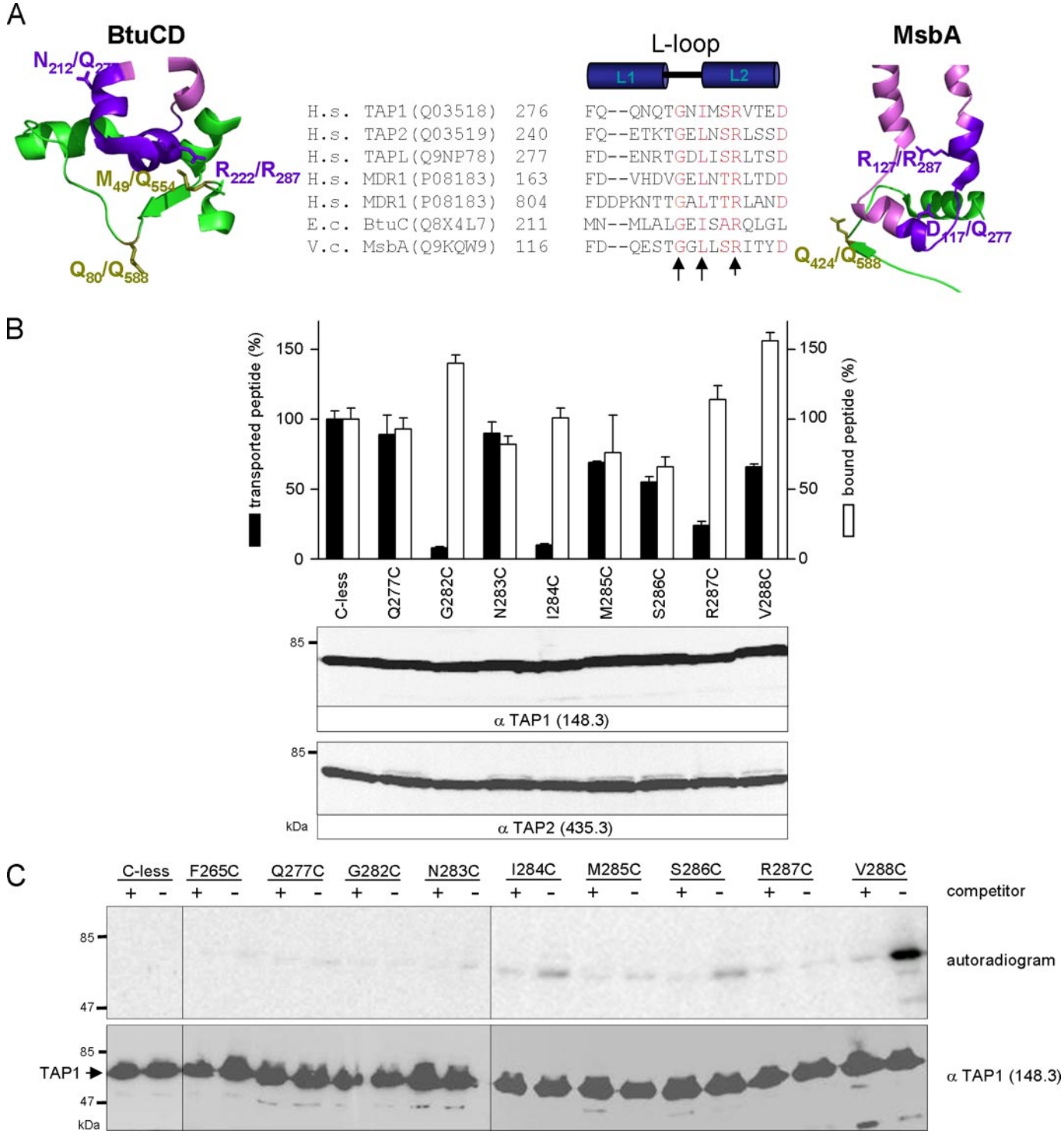

FIGURE 5. **Residues adjacent to the sensor loop are essential for peptide transport.** *A*, structural models of the TMD-NBD interface and sequence alignment of the cytosolic core loop 1. Structures are derived from the x-ray data of BtuCD (21) (PDB 1L7V) and MsbA (20) (PDB 1PF4) and are generated by Pymol (www.pymol.org). The contact region between the TMD (*blue*) and NBD (*green*) is illustrated. Remaining sequences of the TMD are shown in *magenta*. Residues of the L-loop contacting the NBD by hydrogen bonds or van der Waals interactions are shown by side chains and are *numbered* according to the position in the solved structure and the corresponding residue in TAP1. Sequence alignment of the cytosolic core loop 1 with the L-loop or intracellular domain 1 of other ABC transporters was performed with ClustalW (Swiss-Prot accession numbers are depicted). On top, the arrangement of the L1 and L2 helices as found in BtuC is shown. Most conserved residues are marked *red*. An *arrow* labels residues that are identified by cysteine scanning to be essential for peptide transport. *B*, peptide binding (*open bars*) and transport (*filled bars*) of TAP1 mutants. For peptide binding, TAP-containing membranes (60 μg of total protein; TAP1(single cysteine or cysteine-less) combined with TAP2(wt)) were incubated with 1 μM radiolabeled RRYQKSTEL at 4 °C for 15 min. Specific peptide binding to the cysteine-less TAP1/wt TAP2 complex was normalized to 100%. The data and errors were derived from triplicate measurements. Peptide transport was performed with saponin semi-permeabilized insect cells (2.5×10^6 cells) for 3 min at 32 °C in the presence and absence of 10 mM ATP. ATP-specific transport of cysteine-less TAP1/wt TAP2 complex was normalized to 100%. Equal amounts of TAP were confirmed by immunoblotting. *C*, only the C-terminal part of the CCL1 is in contact with the bound peptide. Site-specific oxidative cross-linking of radiolabeled C6-peptide (1.25 μM) in the absence or presence of the competitor peptide RRYQKSTEL (250 μM) with different single cysteine variants and cysteine-less TAP1/TAP2(wt) (0.5 mg of protein) was performed as outlined in Fig. 4*B*. Equal amounts of TAP in each experiment were confirmed by immunoblotting.

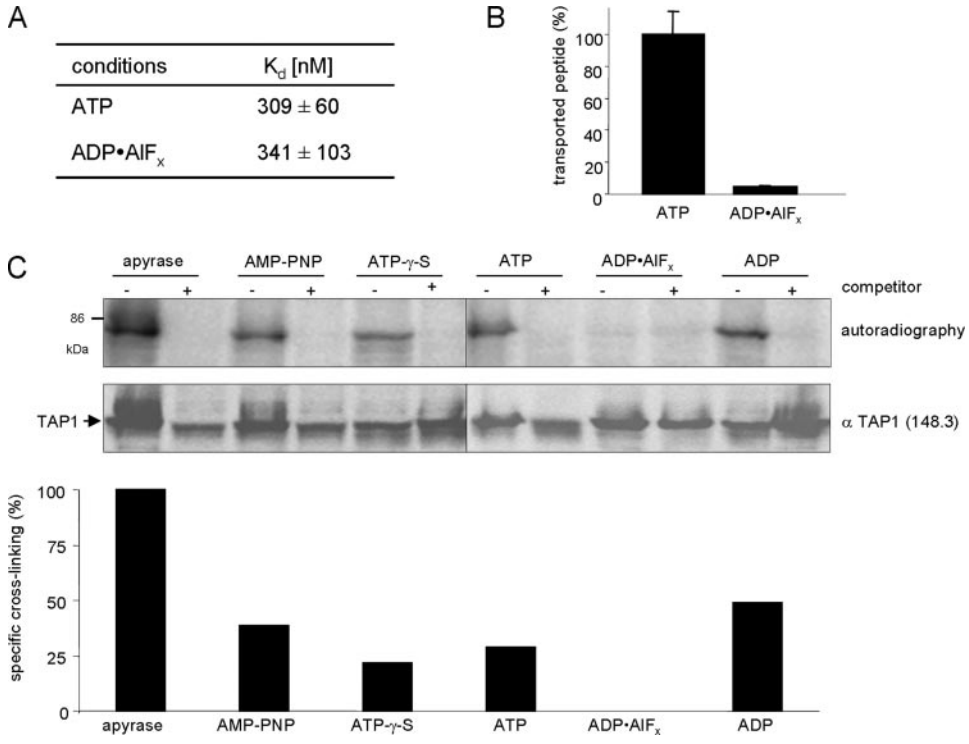

FIGURE 6. **The peptide sensor loop is remodeled during the ATP hydrolysis cycle.** TAP-containing membranes were preincubated with 1 μM RRYQKSTEL and 5 mM ATP in the presence or absence of 2.5 mM AlF$_x$ for 25 min at 27 °C. Afterward, membranes were washed once. *A*, peptide binding affinity. Pre-treated TAP1(V288C)/TAP2(wt) (25 μg of total protein) was incubated with increasing concentrations of radiolabeled RRYQKCTEL (plus 1 mM dithiothreitol) for 15 min at 4 °C. The amount of specifically bound peptide was plotted against peptide concentration and fitted by a Langmuir (1:1) isotherm. *B*, peptide transport. Pre-treated TAP1(V288C)/TAP2(wt) (150 μg of total protein) was incubated with 1 μM of RRYQNSTC$^{(F)}$L (fluorescein-labeled cysteine) in the presence of 5 mM ATP or ADP for 3 min at 32 °C. Transported and glycosylated peptides were purified and detected by fluorescence emission ($\lambda_{ex/em}$ = 485/520 nm). ATP-specific transport of trapped (*ADP·AlF$_x$*) and non-trapped (*ATP*) TAP is depicted. The data and errors were derived from triplicate measurements. *C*, oxidative cross-linking. TAP1(V288C)/TAP2(wt) (500 μg of total protein) was trapped in the ADP·AlF$_4^-$ transition state as described above or incubated with either 3 mM ATP, 3 mM ADP, 3 mM AMPPNP, 3 mM ATPγS, or apyrase (2 units). Afterward, radiolabeled C6-peptide (1.25 μM) was added in the absence or presence of the competitor peptide RRYQKSTEL (250 μM). Cross-linking was induced by adding copper phenanthroline (1 mM). After metal affinity capture of TAP, cross-linked products were analyzed by non-reducing SDS-PAGE and autoradiography. TAP amount was quantified by immunoblotting. The cross-linking intensities (quantified by ImageQuaNT software) were normalized to TAP amounts, and relative specific cross-linking was related to cross-linking in the presence of apyrase as depicted in the *lower panel*.

(22) or F1-type ATPases (23). Derived from x-ray structures of myosin, this ADP-trapped state mimics the pentacovalent phosphorous transition state of ATP hydrolysis (24). In this state, peptide transport but not peptide binding by TAP is inhibited (Fig. 6, *A* and *B*). As shown in Fig. 6*C*, cysteine cross-linking of the single cysteine peptides to residue 288 of TAP1 was observed in the presence of ADP or ATP. In addition, in the presence of the non-hydrolysable ATP-analogues ATPγS and AMPPNP, which do not energize peptide transport (6), peptide cross-linking occurred. Disulfide trapping was most efficient in the absence of nucleotides. Strikingly, if the TAP complex was arrested in the translocation incompetent ADP·AlF$_x$ state, no specific peptide contact to the peptide sensor site was observed. These results demonstrate a structural reorganization of the peptide sensor and transmission interface and an inter-domain cross-talk of the TMD and NBD during ATP hydrolysis.

DISCUSSION

As the key component of the MHC class I peptide-loading complex, TAP translocates proteasomal degradation products into the endoplasmic reticulum lumen. Peptide binding is a key step in the overall TAP transport mechanism and in the selection of epitopes presented by MHC class I molecules (25, 26). Peptide binding to the transmembrane domains of TAP is tightly coupled to ATP hydrolysis by the NBDs (9, 10). However, sterically restricted peptides bound to TAP do not trigger ATP hydrolysis and are not transported. It is an open question how the quality of incoming peptides is checked and transmitted to the ATPase domains to drive peptide translocation.

To identify sites sensing peptides bound to TAP, we modified peptide epitopes by a small chemical protease. The iron-dependent protease has previously been successfully applied to map RNA/DNA-protein interaction sites (27, 28). Based on a hydrolytic mechanism, cleavage is observed when the carbonyl oxygen of the polypeptide chain points perpendicularly to the iron complex facilitating the nucleophilic attack on the carbonyl carbon by the iron-peroxo species (18). Alternatively, short living hydroxyl radicals can abstract a hydrogen from the α-carbon of an amino acid leading to an unstable carbon-centered radical that degrades, forming new blocked termini (18). In both cases, the cleavage is limited to a 1.2-nm distance from the attachment site of the chemical protease (29, 30). The cleavage is very fast and achieved within 10 s (see Fig. 2), and the cutting efficiency (up to 40%) is only limited by a "self-cutting" of the peptide (data not shown).

With the Trojan horse strategy, two TAP1-peptide contact sites have been identified. Based on the size of the less prominent C- and N-terminal fragments (p_C29 and p_N48), one contact site is located to a stretch following TM6 (see Fig. 3*C*). This site overlaps with the peptide-binding pocket derived from peptide photo-cross-linking studies (14). The other peptide contact site was identified at position 290 ± 2 of TAP1 by mass spectrometry and cysteine cross-linking. The peptide contact site is part of the cytosolic core loop 1, which shares some degree of homology with the intracellular domain 1 of MsbA or L-loop of BtuCD.

The iron-chelating peptides cleave only TAP1 but not TAP2. At first, this seems to be in conflict to previous results, showing that the peptide-binding pocket is shared by TAP1 and TAP2 (14). However, asymmetry of both subunits is reflected in different peptide transport specificities of rat TAP2 alleles. TAP

complexes containing the ratTAP2[a] allele are promiscuous in regard to the C-terminal residue of the peptide, whereas TAP containing the rat TAP2[u] allele selects against peptides with C-terminal small polar/hydrophobic or positively charged residues (31, 32). The lack of TAP2 cleavage may also result from improper orientation or steric constraints of the chemical protease in respect to the cleavage site (18).

It is worth mentioning that peptides with the chemical protease attached to positions 6 and 7 showed the highest cleavage efficiency. Interestingly, these positions have only a minor influence on the peptide specificity (11). Therefore we conclude that the transmission interface identified is not involved in the fixation of the peptide in the binding pocket but rather in sensing the bound peptide. The peptide-binding pocket of TAP possesses certain flexibility, because peptides of 8–16 residues are bound with the same affinity and translocated by TAP (5, 33). As demonstrated in this study, TAP uses the same peptide sensor loop for the recognition of peptides, which differ in length and sequence. In addition, these peptides were specifically cross-linked to the single cysteine in the contact site. These data demonstrate (i) that peptides of different sequence and length bind with the same orientation to TAP, and (ii) that the central peptide region, which is distinct from the anchor positions 1–3 and the C terminus, is sensed by the TAP interface.

The identified peptide sensor and transmission interface aligns with the intracellular domain 1 of MsbA or the L2-helix of BtuCD. Biochemical and structural studies showed that these transmembrane loops are in close contact with the Q-loop and the α-helical domain of the NBD (20, 21, 34). Derived from x-ray structures, the Q-loop connects the catalytic domain with the α-helical domain of the NBDs and is involved in structural rearrangement by sensing bound ATP, which is the initial step for dimerization of the NBDs (35). The cysteine-scanning approach supports the function of CCL1 as signal transducer in ABC exporters, because it does not interfere with substrate binding but with substrate transport. Interestingly, the most severe effects in disrupting the tight coupling between peptide binding and transport and the inter-domain communication were found for the most conserved residues in the sensor loop, comprising Gly-282, which seems to function as a helix breaker, and Ile-284 and Arg-287 of TAP1. Both residues are separated by three residues and therefore are on the same face of the α-helix. Together with Val-288, these residues are essential in sensing the bound peptide and interdomain signal transmission. Interestingly, the dual function can also be structurally separated to the sensor region at the C-terminal end and the transmission site upstream.

The peptide contact site is restructured during the ATP hydrolysis cycle. In the nucleotide-free state, the strongest cross-linking between peptide and sensor loop is detected. Binding of nucleotide weakens this interaction, which could resemble a structural rearrangement. For P-glycoprotein such a conformational change by binding AMPPNP could be shown by cryoelectron microscopy of two-dimensional crystals (36). Trapping P-glycoprotein in the ATP hydrolysis transition state by ortho-vanadate, which resembles the same trapped state as AlF_x in myosin (24, 37), induced a further change in structure. Also TAP showed a structural change trapped in the ATP hydrolysis transition state, because direct contact between peptide and the sensor and transmission loop is abolished. This peptide contact region appears to act asymmetrically, because we detected only cleavage in TAP1, but not in TAP2. This finding is in accordance with the functional asymmetry of the EAA motifs (L-loops) found in MalG/F (38). Some mutations in the EAA motif of MalG abrogate maltose uptake, whereas the identical mutations in MalF show only a weak influence on activity. Moreover, these mutations can be suppressed by mutations in the α-helical domain of MalK, the NBD of the maltose permease.

In summary, we propose the following model. The peptide binds to TAP in a fast association step and is anchored at the TAP1-TAP2 interface via the first three N- and last C-terminal residues (7, 11). Subsequently, a slow structural rearrangement of TAP follows, which may resemble the sensing of the bound peptide by the contact loop of TAP1 identified in this study. This conformational change may induce a rearrangement of the TMD-NBD interface, so that the NBDs can dimerize in the presence of ATP, which is a prerequisite for ATP hydrolysis. Altogether 25% of all residues of TAP are involved in reorganization of TAP during peptide binding (8). In the absence of peptides, the NBDs are kept in a conformation, impeding dimer formation and ATP hydrolysis (9). Moreover, an additional ATP- and peptide-dependent conformational change is detected, which may resemble the peptide translocation process (39). Sterically restricted peptides, which still bind to TAP but are not transported (12) and do not stimulate ATP hydrolysis (9), do not allow the conformational change of the contact loop, which is the initial step in interdomain signal transduction. Therefore, the sensor region allows quality control of the bound peptide and enables a tight communication between the TMD (substrate binding) and the NBD (ATP hydrolysis).

Acknowledgments—We thank Eckhard Linker, Gudrun Illig, and Gerhard Spatz-Kümbel for their excellent technical assistance. We are indebted to Ute Bahr for help with the MS analysis of membrane proteins.

Addendum—Shortly before submission of our manuscript, the 3.0-Å crystal structure of a bacterial multidrug ABC transporter Sav1866 from *Staphylococcus aureus* was reported (40). Sav1866 shows significant sequence similarity to the core TAP complex (see Fig. 3). The new structure fully supports our findings on the transmission interface. The peptide sensor loop of TAP1 (CCL1) aligns with the intracellular loop 1. Based on the new structure, the peptide and transmission interface of TAP1 (including Gly-282, Ile-284, Arg-287, and Val-288) connects the coupling helix 1 with the TM3 and is therefore a focal point in the inter-domain communication.

REFERENCES

1. Abele, R., and Tampé, R. (2004) *Physiology* (*Bethesda*) **19,** 216–224
2. Cresswell, P., Ackerman, A. L., Giodini, A., Peaper, D. R., and Wearsch, P. A. (2005) *Immunol. Rev.* **207,** 145–157
3. Higgins, C. F. (1992) *Annu. Rev. Cell Biol.* **8,** 67–113
4. Schmitt, L., and Tampé, R. (2002) *Curr. Opin. Struct. Biol.* **12,** 754–760
5. van Endert, P. M., Tampé, R., Meyer, T. H., Tisch, R., Bach, J. F., and McDevitt, H. O. (1994) *Immunity* **1,** 491–500
6. Meyer, T. H., van Endert, P. M., Uebel, S., Ehring, B., and Tampé, R. (1994) *FEBS Lett.* **351,** 443–447

7. Neumann, L., and Tampé, R. (1999) *J. Mol. Biol.* **294,** 1203–1213
8. Neumann, L., Abele, R., and Tampé, R. (2002) *J. Mol. Biol.* **324,** 965–973
9. Gorbulev, S., Abele, R., and Tampé, R. (2001) *Proc. Natl. Acad. Sci. U. S. A.* **98,** 3732–3737
10. Chen, M., Abele, R., and Tampé, R. (2003) *J. Biol. Chem.* **278,** 29686–29692
11. Uebel, S., Kraas, W., Kienle, S., Wiesmüller, K. H., Jung, G., and Tampé, R. (1997) *Proc. Natl. Acad. Sci. U. S. A.* **94,** 8976–8981
12. Grommé, M., van der Valk, R., Sliedregt, K., Vernie, L., Liskamp, R., Hämmerling, G., Koopmann, J. O., Momburg, F., and Neefjes, J. (1997) *Eur. J. Immunol.* **27,** 898–904
13. Uebel, S., Meyer, T. H., Kraas, W., Kienle, S., Jung, G., Wiesmüller, K. H., and Tampé, R. (1995) *J. Biol. Chem.* **270,** 18512–18516
14. Nijenhuis, M., and Hämmerling, G. J. (1996) *J. Immunol.* **157,** 5467–5477
15. Hayward, M. M., Adrian, J. C., Jr., and Schepartz, A. (1995) *J. Org. Chem.* **60,** 3924–3927
16. Schrodt, S., Koch, J., and Tampé, R. (2006) *J. Biol. Chem.* **281,** 6455–6462
17. Wessel, D., and Flügge, U. I. (1984) *Anal. Biochem.* **138,** 141–143
18. Datwyler, S. A., and Meares, C. F. (2001) *Met. Ions Biol. Syst.* **38,** 213–254
19. Wu, J., and Kaback, H. R. (1996) *Proc. Natl. Acad. Sci. U. S. A.* **93,** 14498–14502
20. Chang, G. (2003) *J. Mol. Biol.* **330,** 419–430
21. Locher, K. P., Lee, A. T., and Rees, D. C. (2002) *Science* **296,** 1091–1098
22. Sankaran, B., Bhagat, S., and Senior, A. E. (1997) *Arch. Biochem. Biophys.* **341,** 160–169
23. Lunardi, J., Dupuis, A., Garin, J., Issartel, J. P., Michel, L., Chabre, M., and Vignais, P. V. (1988) *Proc. Natl. Acad. Sci. U. S. A.* **85,** 8958–8962
24. Fisher, A. J., Smith, C. A., Thoden, J. B., Smith, R., Sutoh, K., Holden, H. M., and Rayment, I. (1995) *Biochemistry* **34,** 8960–8972
25. Uebel, S., and Tampé, R. (1999) *Curr. Opin. Immunol.* **11,** 203–208
26. van Endert, P. M., Saveanu, L., Hewitt, E. W., and Lehner, P. (2002) *Trends Biochem. Sci.* **27,** 454–461
27. Schmidt, B. D., and Meares, C. F. (2002) *Biochemistry* **41,** 4186–4192
28. Datwyler, S. A., and Meares, C. F. (2000) *Trends Biochem. Sci.* **25,** 408–414
29. Rana, T., and Meares, C. (1991) *Proc. Natl. Acad. Sci. U. S. A.* **88,** 10578–10582
30. Ghaim, J. B., Greiner, D. P., Meares, C. F., and Gennis, R. B. (1995) *Biochemistry* **34,** 11311–11315
31. Heemels, M. T., Schumacher, T. N., Wonigeit, K., and Ploegh, H. L. (1993) *Science* **262,** 2059–2063
32. Momburg, F., Roelse, J., Howard, J. C., Butcher, G. W., Hämmerling, G. J., and Neefjes, J. J. (1994) *Nature* **367,** 648–651
33. Koopmann, J. O., Post, M., Neefjes, J. J., Hämmerling, G. J., and Momburg, F. (1996) *Eur. J. Immunol.* **26,** 1720–1728
34. Dalmas, O., Orelle, C., Foucher, A. E., Geourjon, C., Crouzy, S., Di Pietro, A., and Jault, J. M. (2005) *J. Biol. Chem.* **280,** 36857–36864
35. Smith, P. C., Karpowich, N., Millen, L., Moody, J. E., Rosen, J., Thomas, P. J., and Hunt, J. F. (2002) *Mol. Cell* **10,** 139–149
36. Rosenberg, M. F., Velarde, G., Ford, R. C., Martin, C., Berridge, G., Kerr, I. D., Callaghan, R., Schmidlin, A., Wooding, C., Linton, K. J., and Higgins, C. F. (2001) *EMBO J.* **20,** 5615–5625
37. Smith, C. A., and Rayment, I. (1996) *Biochemistry* **35,** 5404–5417
38. Mourez, M., Hofnung, M., and Dassa, E. (1997) *EMBO J.* **16,** 3066–3077
39. Reits, E. A., Vos, J. C., Grommé, M., and Neefjes, J. (2000) *Nature* **404,** 774–778
40. Dawson, R. J., and Locher, K. P. (2006) *Nature* **443,** 180–185
41. Koch, J., Guntrum, R., Heintke, S., Kyritsis, C., and Tampé, R. (2004) *J. Biol. Chem.* **279,** 10142–10147